Facile Preparation of Multifunctionalisable 'Stealth' Upconverting Nanoparticles for Biomedical Applications

Nsubuga, A.; Sgarzi, M.; Zarschler, K.; Kubeil, M.; Hübner, R.; Steudtner, R.; Graham, B.; Joshi, T.; Stephan, H.;

Originally published:

April 2018

Dalton Transactions 47(2018), 8595-8604

DOI: https://doi.org/10.1039/C8DT00241J

Journal Name

ARTICLE

Facile Preparation of Multifunctionalisable 'Stealth' Upconverting Nanoparticles for Biomedical Applications

Received 00th January 20xx,
Accepted 00th January 20xx

DOI: 10.1039/x0xx00000x

www.rsc.org/

Anne Nsubuga,[a¶] Massimo Sgarzi,*[a¶] Kristof Zarschler,[a] Manja Kubeil,[a] René Hübner,[b] Robin Steudtner,[c] Bim Graham,[b] Tanmaya Joshi,*[a] and Holger Stephan*[a]

In memory of Leone Spiccia

Pure hexagonal (β-phase) $NaYF_4$-based hydrophobic upconverting nanoparticles (UCNPs) were surface-modified with *o*-phospho-L-threonine (OPLT), alendronic acid, and PEG-phosphate ligands to generate water-dispersible UCNPs. Fourier-transform infrared (FTIR) spectroscopy was used to establish the presence of the ligands on the UCNP surface. These UCNPs exhibit great colloidal stability and a near-neutral surface at physiological pH, as confirmed by dynamic light scattering (DLS) and zeta potential (ζ) measurements, respectively. The particles also display excellent long-term stability, with no major adverse effect on the size of UCNPs when kept at pH 7.4. Upon exposure to human serum, PEG-phosphate- and alendronate-coated UCNPs showed no formation of biomolecular corona, as confirmed by SDS-PAGE analysis. The photophysical properties of water-dispersible UCNPs were investigated using steady-state as well as time-resolved luminescence spectroscopy, under excitation at ca. 800 nm. The results clearly show that the UCNPs demonstrate bright upconversion (UC) luminescence. Furthermore, the presence of reactive groups on the NPs, such as, free amine group in alendronate-coated UCNPs, enables further functionalisation of UCNPs with, for example, small molecules, peptides, proteins, and antibodies. Overall these protein corona resistant UCNPs show great biocompatibility and are worthy of further investigation as potential new biomaging probes.

INTRODUCTION

Lanthanide-doped upconverting nanoparticles (UCNPs) are a special class of photoluminescent nanomaterials (NMs) that can sequentially absorb two or more near-infrared (NIR) photons in order to emit higher energy photons.[1-4] Thanks to their low toxicity,[5, 6] photostability,[7] and their ability to generate long-lived (µs up to ms range) sharp and intense anti-Stokes luminescence,[2, 8] UCNPs are emerging as an important class of fluorescent imaging probes.[9] UCNPs typically consist of an inorganic host matrix (e.g., $NaYF_4$), co-doped with an activator (e.g., Er^{3+}, Tm^{3+}, Ho^{3+}) and either Yb^{3+} or Nd^{3+} ions as the sensitiser. Their spectral properties can be easily tuned not only by varying the dopant Ln^{3+} ions but also their relative proportions. Furthermore, the excitation of UCNPs by means of low energy NIR radiation allows to exploit the NIR-1 optical transparency window (650–950 nm), where water and tissue absorption is minimal,[10, 11] resulting in higher penetration depths[12] and reduced photodamage.[13] This attractive property, coupled with their chemical robustness and higher signal-to-noise ratio due to reduced background autofluorescence,[14] makes them one family of NMs offering excellent prospects of biomedical applications.[2, 15]

Synthesis of UCNPs is usually carried out in high-boiling non-aqueous solvents,[8, 16-23] and results in nanocrystals capped with hydrophobic organic ligands.[8, 17, 19-23] Consequently, for their application as biomedical tools, UCNPs need to be made water-dispersible and colloidally stable whilst retaining their optical properties.[24-26] It is fairly challenging to prepare very small hydrophilic UCNPs exhibiting high colloidal stability under complex biological conditions.[4, 22, 26, 27] Moreover, the toxicity, immunological response and pharmacokinetic behaviour of UCNPs, and NMs, in general,[25] can be tremendously affected by their size, shape and surface properties, including charge and composition.[28-32] Upon intravenous administration, NMs enter the systemic circulation

[a] Institute of Radiopharmaceutical Cancer Research, Helmholtz-Zentrum Dresden-Rossendorf, Bautzner Landstraße 400, 01328 Dresden, Germany. Email: m.sgarzi@hzdr.de, t.joshi@hzdr.de, h.stephan@hzdr.de
[b] Institute of Ion Beam Physics and Materials Research, Helmholtz-Zentrum Dresden-Rossendorf, Bautzner Landstraße 400, 01328 Dresden, Germany.
[c] Institute of Resource Ecology, Helmholtz-Zentrum Dresden-Rossendorf, Bautzner Landstraße 400, 01328 Dresden, Germany
[d] Monash Institute of Pharmaceutical Sciences, Monash University, Parkville, VIC 3052, Australia.
¶ These authors contributed equally to this work.

Electronic Supplementary Information (ESI) available: Digital photographs of the colloidal dispersions of UCNPs after excitation at λ = 793 nm, SDS-PAGE analysis of the biomolecular corona formation on OPLT-coated UCNPs, TLC analysis of alendronate-coated UCNPs after FITC coupling. See DOI: 10.1039/x0xx00000x

and are distributed throughout the body via the bloodstream. Within the vascular system, the complex biological environment encountered by these nanoparticles contains a wide range of substances, which can lead to their destabilisation, aggregation and degradation.[29, 33] Furthermore, depending on their surface decoration, biological macromolecules such as serum proteins and lipids can bind to the NMs non-specifically, leading to the formation of the so-called 'biomolecular corona'.[34, 35] This differential adsorption of serum constituents results in recognition as well as uptake of NMs by mononuclear phagocytic cells, in their elimination from the blood circulation and in their accumulation in the organs of the mononuclear phagocyte system (MPS).[36, 37] This resulting suboptimal tissue distribution and pharmacokinetic profile of the NMs is, in fact, one of the major obstacles to their medical application and translation to the clinic.[38-40]

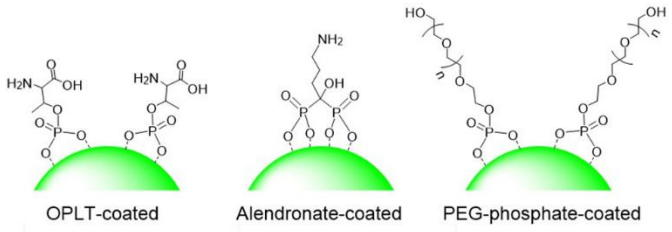

Figure 1. Water-dispersible UCNPs studied in this work.

Manufacturing of NMs with surface coatings that can prevent biomolecular corona formation is an ambitious objective of current research.[41] In this regard, surface modification with hydrophilic, neutral-charged polymers, e.g. polyethylene glycol (PEGylation), represents the most widely employed procedure to inhibit the undesirable adsorption of biological macromolecules by using steric repulsion effects.[42-44] However, PEGylation can substantially increase the hydrodynamic diameter (D_h) of NMs and is thus unsuitable for surface engineering of rapidly circulating entities.[45] Recently, we and others have explored the use of zwitterionic coatings to control the extent of production of biomolecular corona.[46-50] For instance, we showed that surface coating of hydrophobic ultrasmall iron oxide nanoparticles (USPIONs) with amphiphilic zwitterionic polymers can help to greatly reduce the extent of protein corona formation.[49] Similarly, water-dispersible USPIONs can also be conferred 'stealth' properties without any substantial increase in particle size by tethering the low-molecular weight zwitterionic sulfobetaine derivatives to their surface,[48] thereby also providing sites for grafting a multitude of other functionalities onto the NM surface.

As for the USPIONs, in this work, we investigate the surface modification of UCNPs with the low-molecular weight zwitterionic coating materials to render them water-soluble, but with a view to generate multifunctional entities showing reducing protein-UCNP interactions. Owing to the high upconversion efficiency of β-$NaYF_4$ host matrix systems,[51] β-$NaYF_4$:Nd^{3+}/Yb^{3+}/Er^{3+} (1/20/2%)@$NaYF_4$:Nd^{3+} (25%) core-shell UCNPs, excitable at both 793 nm and 976 nm, have been chosen for investigation in this work. Very recently, we have reported a reliable synthetic method for rapid production of such oleate (OA)-coated monodispersed UCNPs (< 10 nm).[52] The UCNPs synthesised as described above have no inherent aqueous dispersibility. Herein, we report on the synthetic methodology to confer them water-dispersibility, biocompatiblity and functionalisability. Previous studies have shown that phosphates and phosphonates have strong binding affinity for the Ln^{3+} ions.[53-58] Based on this property, we now investigate the use of zwitterionic *o*-phospho-L-threonine (OPLT), alendronic acid, and PEG-phosphate as surface anchoring ligands to produce hydrophilic UCNPs, ready for incorporating multiple modalities. With a view to developing materials suitable for biological applications, we performed the photophysical characterisation of the resulting water-dispersible UCNPs and examined their ability to resist serum protein adsorption.

RESULTS AND DISCUSSION

Synthesis and characterisation of water-dispersible UCNPs

Sub-10 nm, β-$NaYF_4$:Nd^{3+}/Yb^{3+}/Er^{3+} (1/20/2%)@$NaYF_4$:Nd^{3+} (25%) core-shell UCNPs, excitable at both 793 and 976 nm, were prepared using our recently reported one-pot co-precipitation method.[52] Employing this method, it was possible to generate high-quality nanocrystals with narrow size distributions in much shorter reaction time than, for example, the other classical co-precipitation and thermal decomposition methods.[8, 19-23] Dynamic light scattering (DLS) analysis revealed an average size of ca. 9 nm for the UCNPs. The as-synthesised UCNPs, however, are capped with hydrophobic oleate ligands, and are only dispersible in non-polar solvents, such as hexane, cyclohexane, or chloroform.[52] To generate water-dispersible UCNPs suitable for biological application, oleate ions on the surface were replaced with one of the three strong binding ligands, *o*-phospho-L-threonine (OPLT), PEG-phosphate or alendronate, via nitrosonium tetrafluoroborate $NOBF_4$-mediated two-step ligand exchange process (Figure 2).[59] Here, nitrosonium cations act as strong oxidants and vigorously react with the nanocrystal surface, stripping the originally anchored oleate ligands from the nanocrystal surface.[60] The BF_4^- ions, on the other hand, have a weak interaction with the UCNP surface,[59] and conferred hydrophilic character to the UCNPs by allowing their dispersion into dimethylformamide (DMF) for further chemistry to be carried out.[59] The secondary surface modification of BF_4^--coated UCNPs with OPLT, PEG-phosphate, or alendronate ligands was subsequently achieved by the slow addition of UCNPs (dispersion in DMF) to the basic solution of respective capping agents while stirring the dispersions vigorously (to facilitate the ligand exchange). The water-dispersible OPLT-, PEG-phosphate-, and alendronate-coated UCNPs were purified by spin ultrafiltration.

It was possible to monitor the surface modification process by following the changes in the Fourier Transform Infrared (FTIR) spectra of the UCNPs (Figure 3).[59] The FTIR spectrum of as-synthesised OA-coated UCNPs displayed strong symmetric and asymmetric C-H stretching vibrations at 2852 cm^{-1} and 2922

cm^{-1}, respectively, which are assigned to the alkyl chain of OA ligands. In addition, a peak at 3006 cm^{-1} corresponding to =C-H stretch, and bands at 1552 cm^{-1} and 1463 cm^{-1}, ascribable to the symmetric and asymmetric stretching vibration of the carboxylate (COO^-) group bound to the UCNP surface, were also observed. FTIR spectra of BF_4^--coated UCNPs, on the other hand, shows disappearance of these bands, alongside the appearance of new peaks at 1067 cm^{-1} and 1667 cm^{-1}, assignable to BF_4^- anions and C=O stretching vibrations of the DMF solvent molecules, respectively.[59] From these spectral changes, it was reasonably concluded that after $NOBF_4$ treatment, oleate ligands previously anchored to the UCNP surface were successfully replaced by BF_4^- anions.

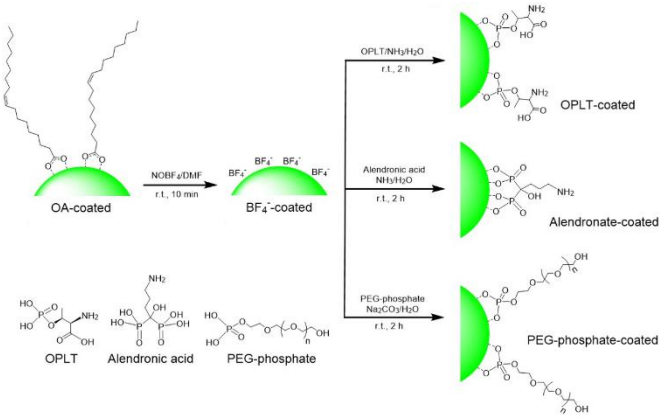

Figure 2. Schematic representation of $NOBF_4$-mediated two-step ligand exchange process for replacing the oleate ions on the surface of hydrophobic UCNPs with *o*-phospho-l-threonine (OPLT), PEG-phosphate or alendronate ligands.

As already reported by Dong et al.,[59] the BF_4^- ions do not have a very strong affinity for the positively charged UCNP surface. In comparison, phosphates and phosphonates can bind strongly to the trivalent rare-earth ions.[61] Taking advantage of this difference in the binding affinity, we subsequently coated the UCNPs with OPLT, PEG-phosphate or alendronate ligands, producing NPs with high aqueous dispersibility (*vide infra*). Once again, FTIR spectroscopy confirmed the presence of OPLT, PEG-phosphate or alendronate ligands on the UCNP surface (Figure 3). For OPLT-UCNPs, the FTIR spectrum showed the presence of the characteristic bands within the region 1300–760 cm^{-1} corresponding to the stretching vibrations of phosphate functional groups. Furthermore, the vibrational bands at 1634 cm^{-1} and 1521 cm^{-1}, assigned to the carboxylic acid and the primary amine functionalities, respectively, were present. Likewise, PEGylated UCNPs exhibited a strong band at 1103 cm^{-1} related to the phosphate group on the UCNP surface, together with –CH stretching vibrations between 3000–2850 cm^{-1}. The FTIR spectrum of alendronate-coated UCNPs showed the P–O stretching region (1052–956 cm^{-1}), indicating the presence of phosphonate groups on the UCNP surface. Moreover, a band at 1560 cm^{-1} was visible in the spectrum, which was associated with the –NH bending vibration and confirmed the presence of amine functionalities in the UCNPs. In the FTIR spectra of all the UCNPs, a broad vibration band centred at ca. 3300 cm^{-1} was also observed due to the OH stretching and presence of water, while the characteristic bands for BF_4^- anions disappeared after the completion of the secondary ligand exchange process.

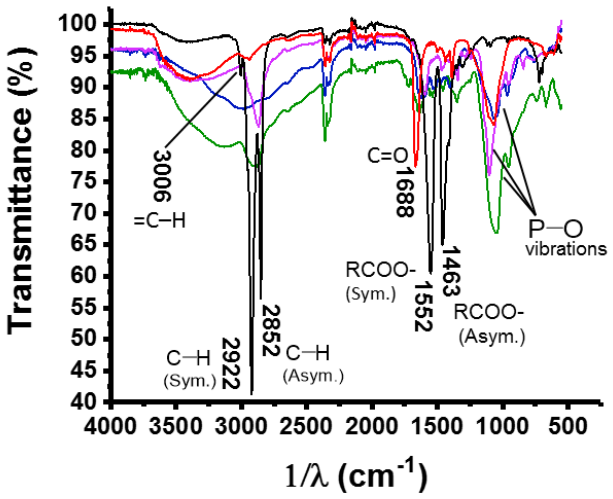

Figure 3. ATR-FTIR spectra of OA- (black solid trace), BF_4^--(red solid trace), OPLT- (azure solid trace), PEG-phosphate- (violet solid trace), and alendronate-coated (green solid trace) $NaYF_4$:Nd^{3+}/Yb^{3+}/Er^{3+} (1/20/2%)@$NaYF_4$:Nd^{3+}(25%) core-shell UCNPs.

Comparison of NP sizes determined by TEM and DLS analysis revealed that the ligand exchange process did have a small effect on the size of the UCNPs in solution (Figure 4 and Table 1). DLS measurements indicated a minor increase in the size of UCNPs, with a mean hydrodynamic diameter (D_h) of ca. 12 nm for OPLT- and alendronate-coated particles, and a slightly larger D_h of 14.2 nm for PEG-phosphate-coated UCNPs, presumably due to the longer PEG chain length and its interaction with the solvated water molecules.[48] That the surface modification occurrs without any loss of monodispersity is supported by the DLS analysis (Table 1). Under physiological conditions, the UCNPs also displayed excellent dispersibility in PBS and in fetal bovine serum (FBS) (Figure S1 shows representative photographs of aqueous dispersions of UCNPs).

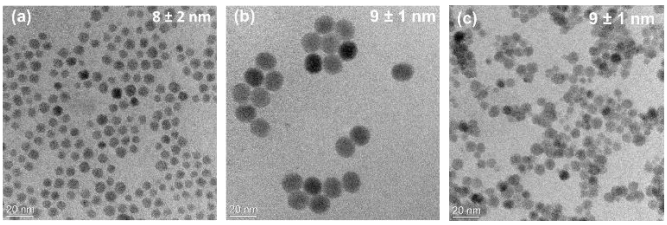

Figure 4. Bright-field TEM images of (a) alendronate-, (b) PEG-phosphate-, and (c) OPLT-coated $NaYF_4$:Nd^{3+}/Yb^{3+}/Er^{3+} (1/20/2%)@$NaYF_4$:Nd^{3+}(25%) core-shell UCNPs. The relative ratio of dopants in the NPs is given as mol%, as obtained by inductively coupled plasma mass spectrometry (ICP-MS) analysis on the OA-coated hydrophobic UCNPs.

Long-term colloidal stability of the hydrophilic UCNPs was probed by measuring the D_h of OPLT-, PEG-phosphate- and alendronate-coated UCNPs in water at pH 7.4, over a period of

up to 28 days after surface modification (Table 1). The hydrophilic UCNPs formed stable colloidal dispersions, and largely remained unaggregated for up to three weeks, when kept at this pH. The D_h of the hydrophilic UCNPs varied very little over this period, not increasing beyond ca. 13–16 nm.

Table 1. DLS particle size distributions (D_h) for OPLT-, alendronate-, and PEG-phosphate-coated $NaYF_4:Nd^{3+}/Yb^{3+}/Er^{3+}$ (1/20/2%)@$NaYF_4:Nd^{3+}$(25%) core-shell UCNPs, measured in water at pH 7.4.

UCNP samples	Particle size (D_h) in nm (PDI)[a]				
	as synthesised	+3 days	+7 days	+21 days	+28 days
OPLT-coated	12.5 ± 2.3 (0.21)	12.6 ± 2.2 (0.25)	12.9 ± 2.2 (0.25)	13.4 ± 3.7 (0.24)	13.8 ± 3.7 (0.48)
Alendronate-coated	12.2 ± 1.8 (0.19)	12.5 ± 2.1 (0.19)	12.7 ± 2.8 (0.18)	13.2 ± 1.2 (0.19)	13.6 ± 5.2 (0.42)
PEG-phosphate-coated	14.2 ± 5.6 (0.34)	14.4 ± 6.4 (0.39)	14.6 ± 6.9 (0.37)	16.1 ± 6.1 (0.36)	16.4 ± 6.1 (0.49)
OA-coated[b]	9.3 ± 1.1 (0.10)	9.5 ± 1.1 (0.12)	9.8 ± 1.1 (0.13)	9.8 ± 1.8 (0.12)	9.9 ± 1.8 (0.13)

[a] Particle size (D_h) correspond to volume-weighted size distributions, and PDI = polydispersity index. [b] The measurements were performed using NP solution in cyclohexane.

As the overall surface charge of NPs is a key contributing factor to their solution stability, their susceptibility to aggregation and precipitation, as well as to their protein binding behaviour *in vivo*, zeta potential (ζ) of the hydrophilic UCNPs was also measured over the pH range 3.5–11.5 (Table 2). At pH 7.4, the zeta potential for the UCNPs was in the range of -6.3 to -14.3 mV, which confirms their overall near-neutral surface at physiological pH.[62] The zeta potential for all the three UCNPs becomes less negative with decreasing pH due to the protonation of some of the anionic groups (carboxylate/phosphate/phosphonate) present in OPLT, PEG-phosphate and alendronate capping ligands. As expected, the OPLT-coated UCNPs display a zwitterionic behaviour with the zeta potential reaching a value of 4.5 mV at pH 3.5. (ζ = 0 mV at pH 5.1). Despite their low surface charge at pH 7.4, the UCNPs display colloidal stability (*vide supra*) due to the strong steric stabilisation ascribable to non-DLVO repulsive forces.[63, 64]

Table 2. Zeta potential (ζ) of OPLT-, alendronate-, and PEG-phosphate-coated $NaYF_4:Nd^{3+}/Yb^{3+}/Er^{3+}$ (1/20/2%)@$NaYF_4:Nd^{3+}$(25%) core-shell UCNPs, measured over the pH range 3.5–11.5.

pH	Zeta potential (ζ) in mV		
	OPLT-coated	Alendronate-coated	PEG-phosphate-coated
3.5	4.6	N.D.	-11.3
5.1	0	-5.2	-10.6
7.4	-6.3	-14.3	-10.8
8.4	-11.1	-19.3	-13.1
11.5	-20.4	-26.0	-20.1

Upconversion luminescence properties

The upconversion ability of OPLT-, PEG-phosphate-, and alendronate-coated UCNPs was retained in water upon excitation at λ = 800 nm (Figures 5, S1 and S2). The upconversion emission spectra of all the three UCNPs are characterised by the emission bands of Er^{3+} ions: three intense bands are present, which are centred at λ = 528, 549 and 674 nm and correspond to $^2H_{11/2} \rightarrow {}^4I_{15/2}$, $^4S_{3/2} \rightarrow {}^4I_{15/2}$, and $^4F_{9/2} \rightarrow {}^4I_{15/2}$ transitions respectively.

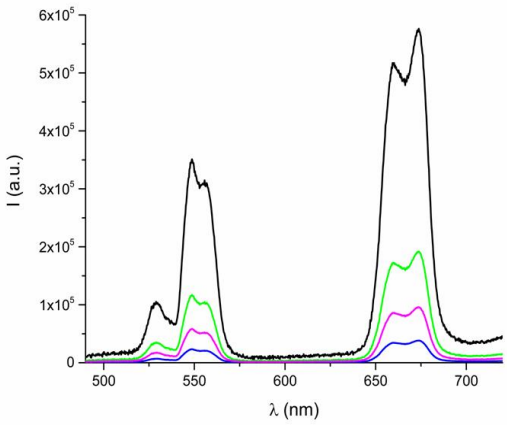

Figure 5. UC emission spectra of OA- (black solid trace), OPLT- (azure solid trace), PEG-phosphate- (violet solid trace), and alendronate-coated (green solid trace) $NaYF_4:Nd^{3+}/Yb^{3+}/Er^{3+}$ (1/20/2%)@$NaYF_4:Nd^{3+}$(25%) core-shell UCNPs. For the hydrophilic UCNPs, spectra were recorded in water, whereas the measurements on the OA-coated UCNPs were performed in cyclohexane. All the spectra were registered under λ = 800 nm excitation with a fs pulsed laser.

These results are consistent with energy transfer upconversion (ETU)[2] processes involving Nd^{3+} (primary sensitiser), Yb^{3+} (secondary sensitiser) and Er^{3+} ions (activator) as described in Figure 6. To note, the spectra were registered by using the same concentration of NPs (6 mg/mL) and the same instrumental settings (see Experimental Section). Taking OA-coated UCNPs as a reference, it can be noticed that the UC intensity dropped by 33% in the case of alendronate-coated UCNPs, while a decrease to 16% and 6.6% was observed for PEG-phosphate- and OPLT-coated UCNPs, respectively. Surprisingly, we did not observe any change in the relative ratios of the integrated intensity for the green and red emission bands (I_G/I_R), which remained constant for all the UCNPs ($I_G/I_R \approx 0.52$), independent of the dispersing medium (Figure 5). Usually in the erbium-doped UCNPs, the OH groups

promote multiphonon relaxation of the $^4I_{11/2} \rightarrow {}^4I_{13/2}$ and $^2H_{11/2}/{}^4S_{3/2} \rightarrow {}^4F_{9/2}$ transitions (Figure 6), which favour the population of the $^4F_{9/2}$ level, causing a decrease of I_G/I_R ratio.[65] The unusual behaviour presented by the hydrophilic UCNPs developed in this work, therefore, suggests that water molecules cannot reach the Er^{3+} excited states into the NP core. This hypothesis is also supported by invariance in the UC lifetimes for the $^2H_{11/2}/{}^4S_{3/2} \rightarrow {}^4F_{9/2}$ transitions in cyclohexane and in water (*vide infra*). The decrease of the emission intensity for the hydrophilic UCNPs (Figure 5) can be ascribed to the quenching of Nd^{3+} excited states by water molecules[66] and surface ligand oscillators.[67]

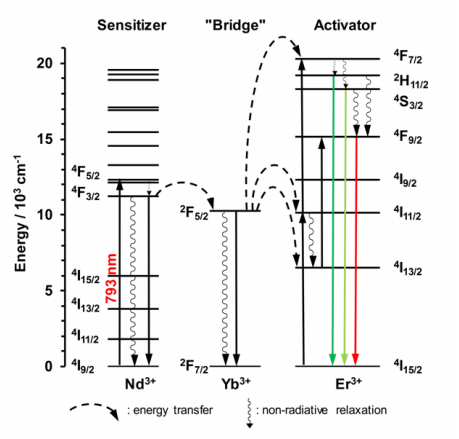

Figure 6. Schematic representation of the UC mechanism in $NaYF_4:Nd^{3+}/Yb^{3+}/Er^{3+}$ (1/20/2%)@$NaYF_4:Nd^{3+}$(25%) UCNPs studied in this work, following their λ = 793 nm laser excitation.

Interestingly, upon laser excitation at λ = 793 nm, the UC lifetime decays for all the NPs studied in this work were non-exponential but hyperbolic (Figure 7). Such behaviour is typical for persistent phosphors.[68, 69] Upconverting persistent luminescence (UCPL) is usually observed in composite systems exploiting the excitation energy transfer between the upconverters (donors) and the persistent phosphors (acceptors).[20, 70-73] To the best of our knowledge, this is the first case of persistent luminescence in non-composite UCNPs, in the absence of persistent phosphors. One possible explanation involves the role of the Nd^{3+} ions, which act as hole traps.[74] The ETU processes that cause the excitation of the Er^{3+} ions also create holes, which can be captured by the Nd^{3+} traps. These holes subsequently undergo a series of detrapping-retrapping cycles before being thermally released from the traps. This allows the excited Er^{3+} ions to radiatively deactivate to the ground state, yielding the long-lasting luminescence.

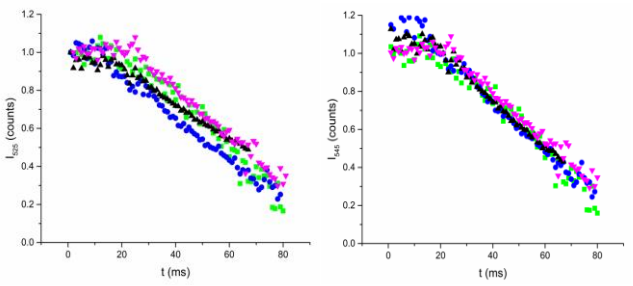

Figure 7. Normalised curves for UC emission luminescence decay for OA- (black up-pointing triangles), OPLT- (azure circles), PEG-phosphate- (violet down-pointing triangles), and alendronate-coated (green squares) $NaYF_4:Nd^{3+}/Yb^{3+}/Er^{3+}$ (1/20/2%)@$NaYF_4:Nd^{3+}$(25%) core-shell UCNPs. Spectra were measured in water (hydrophilic UCNPs) or cyclohexane (OA-coated UCNPs), and were registered at λ = 525 (left) and 545 nm (right), after λ = 793 nm laser excitation.

The decay trends corresponded to a high retrapping rate regime, and were fitted according to the following equation

$$I = \frac{I_0}{(1+\gamma t)^n} \qquad (1)$$

where I_0 is the initial intensity, γ depends on the density of the traps, on the population of trapped electrons at t = 0 and on the detrapping rate, and n depends on the material.[68] In our case, for all the three UCNP samples, value of n obtained from the fits varied between 0.52 and 1.06 (Table 3); no significant difference in n values were registered between hydrophobic and hydrophilic UCNPs ($0.52<n<0.59$), except for OPLT-coated ones, which presented a higher value (n = 1.05) and consequently a faster luminescence decay.

Table 3. Value of n for OA-, OPLT-, PEG-phosphate-, and alendronate-coated $NaYF_4:Nd^{3+}/Yb^{3+}/Er^{3+}$ (1/20/2%)@$NaYF_4:Nd^{3+}$(25%) core-shell UCNPs, upon laser excitation at λ = 793 nm. The UC decay curves of Er^{3+} ions were collected at λ = 525 ($^2H_{11/2} \rightarrow {}^4I_{15/2}$) and 545 nm ($^4S_{3/2} \rightarrow {}^4I_{15/2}$).

UCNP samples	Value of *n*	
	525 nm	545 nm
OPLT-coated	1.05	1.06
Alendronate-coated	0.55	0.57
PEG-phosphate-coated	0.55	0.56
OA-coated	0.52	0.59

Interaction of water-dispersible UCNPs with serum components

We investigated serum protein-UCNP interactions for the OPLT-, PEG-phosphate-, and alendronate-coated UCNPs using sodium dodecyl sulfate-polyacrylamide gel electrophoresis (SDS-PAGE). For this, the UCNPs were incubated with different concentrations of human serum for 1 h at 37 °C. The UCNP-associated proteins were separated from the supernatant serum by centrifugation, followed by extensive washing with PBS in order to remove proteins with low affinity for the UCNP surface. Finally, serum components retained on the UCNP surface were detached and denatured by incubating for 5 min at 95 °C in Laemmli sample buffer and subjected to 1D SDS-PAGE analysis, followed by visualisation of protein bands by staining with a colloidal Coomassie G-250 dye.

For the PEG-phosphate- and alendronate-coated UCNPs, exposure to human serum resulted in almost no adsorption of serum proteins on to the UCNP surface, even at high serum concentrations, as hardly any protein bands could be visualised for both the UCNPs (Figure 8a and b). This, however, is in clear contrast to the gel for serum-exposed OPLT-coated UCNPs (Figure 8c), where several distinct bands corresponding to UCNP surface-associated serum proteins were observed. This suggests significant biomolecular corona formation for OPLT-coated UCNPs. However, the composition of this corona did not appear to alter dramatically upon increasing the serum concentration, and only lead to an increase in the amount of the proteins adsorbed.

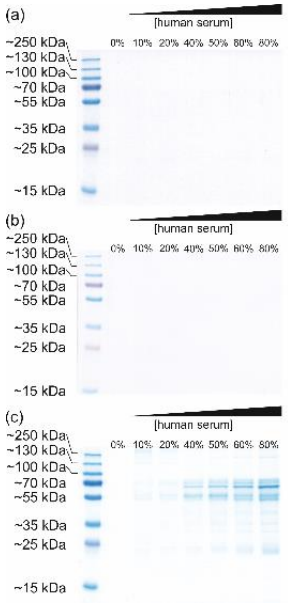

Figure 8. SDS-PAGE analysis of the serum protein absorption on hydrophilic UCNPs. UCNP-associated serum proteins were isolated after incubation of (a) alendronate-, (b) PEG-phosphate-, or (c) OPLT-coated $NaYF_4:Nd^{3+}/Yb^{3+}/Er^{3+}$ (1/20/2%)@$NaYF_4:Nd^{3+}$(25%) core-shell UCNPs with 0–80% of human serum for 1 h at 37 °C.

The substantial biomolecular corona formed on the OPLT-coated UCNPs is rather unexpected as such zwitterionic coatings have previously been found to suppress the nonspecific adsorption of biomolecules to the NM surfaces.[46] One possible explanation for this finding is that the dissociation of OPLT ligands from the NM surface occurs when the NMs are exposed to human serum.[33] In order to investigate the role of serum enzymes and complementary factors in this coating disintegration, we repeated the experiments, but using heat-inactivated human serum (Figure S3a) and lowering the incubation temperature to 4 °C instead of 37 °C (Figure S3b). It is evident from Figure S3 that serum exposure at 4 °C reduced the non-specific adsorption of proteins onto the UCNPs surface up to a certain degree. Moreover, heat inactivation of serum prior to UCNP exposure also had a marginal effect on the biomolecular corona composition.

The composition of the biomolecular corona can be affected by various physicochemical parameters, such as NM size and shape as well as their surface chemistry, charge and coating.[37, 75] Furthermore, the degree of biomolecule coverage and the composition of the biomolecules adsorbed on the NM surface depend on the temperature at which the corona is formed.[76, 77] For example, Mahmoudi *et al.* showed that even subtle changes in temperature can considerably influence the composition of the formed biomolecular corona as well as the affinity of different biomolecules for the NM surface.[77] The differences between the corona composition for the OPLT-coated UCNPs incubated with human serum at 4 °C and 37 °C, respectively, are in accordance with the above-mentioned findings.

Dye functionalisation of alendronate-coated corona-resistant UCNPs

Next, we also investigated the possibility of tethering different functionalities to the protein corona-resistant alendronate-coated UCNPs (*vide supra*). Direct coupling of alendronate-coated UCNPs with fluorescein isothiocyanate (FITC) was attempted with a view to test the accessibility of terminal amine group on the alendronate ions for subsequent conjugation reactions (Figure 9).

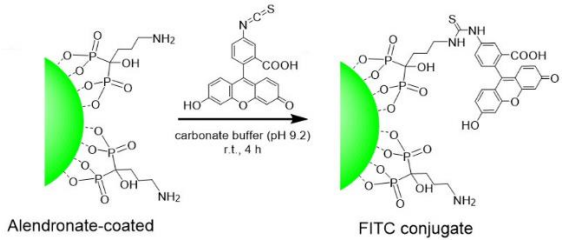

Figure 9. Conjugation of fluorescein isothiocyanate (FITC) to alendronate-coated $NaYF_4:Nd^{3+}/Yb^{3+}/Er^{3+}$ (1/20/2%)@$NaYF_4:Nd^{3+}$(25%) core-shell UCNPs.

After room temperature reaction of alendronate-coated UCNP (2 mg) with 5, 10 or 20 nmol FITC, respectively, the samples were purified by spin ultrafiltration using 10 kDa MW cut-off centrifuge tube filters. First indication on the successful coupling of FITC to the alendronate-coated UCNPs was obtained from thin layer chromatography (TLC) analysis of the UCNP samples taken before (Figure S4a) and after purification (Figure S4b). TLC was performed using glass microfiber chromatography paper impregnated with a silica gel (iTLC-SG) as stationary phase and a 1:2 (v/v) mixture of NH_4OAc (2 M)/MeOH as mobile phase. On this TLC system, hydrophilic UCNPs (R_f = 0) are well-separated from the unbound FITC (R_f = 1). Detection of strong fluorescein emission from the UCNP sample taken after purification suggested that the dye was linked to the alendronate-coated UCNPs. This was further corroborated by the presence of characteristic absorption band, centred around λ = 475 nm, and the emission maxima at λ = 525 nm for the linked fluorescein unit (λ_{ex} = 470 nm), in UV/Vis absorption and photoluminescence spectra, respectively (Figure 10). As expected, the coupling efficiency

depends on the FITC concentration used for the reaction, with a higher dye concentration resulting in higher loading of the dye onto the UCNP surface.

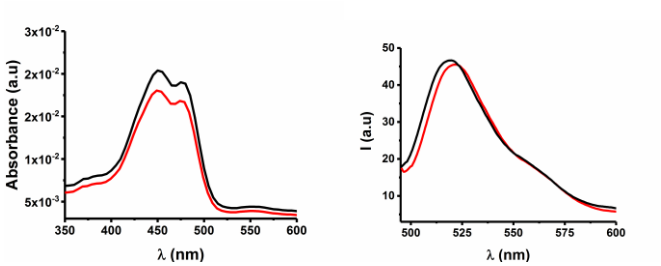

Figure 10. Electronic absorbance (left) and emission spectra (right) of alendronate-coated UCNPs after coupling reaction with FITC. The red trace shows the spectrum for FITC-coupled UCNPs, whereas the spectrum for the free FITC is shown in black.

Conclusions

Water dispersible β-phase $NaYF_4$-based UCNPs, capped with OPLT, PEG-phosphate, and alendronate ligands, have been synthesised by a facile two-step ligand exchange method. TEM and DLS analysis showed that, upon surface modification, the UCNPs do not undergo a significant change in their size (D_h = 12.5–16 nm) and morphology. All the three surface coatings generate UCNPs with high long-term colloidal stability and a close to neutral surface charge at physiological pH. The PEG-phosphate- and alendronate-coated UCNPs also show great resistance to protein corona formation, even when exposed to high serum concentrations. More importantly, the UCNPs retain their photophysical properties and show efficient UC luminescence under irradiation at 793 nm. Moreover, the presence of reactive amine groups on the surface of alendronate coated UCNPs allows for easy conjugation of (radio)chelators, dyes, antibodies and other biomolecules to the UCNP surface. Our future research will focus on understanding the bio-distribution of these UCNPs, which will ultimately prove useful in establishing their potential for biomedical applications.

EXPERIMENTAL SECTION

Materials

Alendronic acid and PEG-phosphate (synthesised using polyethylene glycol of M_n=1000) were synthesised following the literature procedures.[58, 78] The characterisation data were in agreement with those previously reported for the compounds. *O*-phospho-L-threonine (OPLT) (99.9%) was purchased from Sigma Aldrich. Therminol® 66 (T66) was supplied by FRAGOL GmbH (Mülheim, Germany, product number: 2600267). All other chemicals and solvents were of reagent or analytical grade, and were used as received without further purification.

Instrumentation and methods

Dynamic Light scattering (DLS) and zeta potential measurements on UCNPs were performed using Malvern Zetasizer Nano ZS Instrument with a He-Ne laser (λ = 632 nm). Measurements were conducted at 25 °C, with a detection angle of 173°, and the data was processed by means of the Zetasizer software (version 7.12). The measurements were done in triplicate and sample solutions were passed through a nylon syringe filter (0.2 μm) prior to the measurements.

Transmission electron microscopy (TEM) images were acquired using an image C_s-corrected FEI Titan 80-300 electron microscope, operating at an accelerating voltage of 300 kV. Samples were prepared by drop-casting NP dispersions on carbon-coated TEM grids followed by drying in air.

Infrared spectra were acquired on a Nicolet iS5 FT-IR spectrometer, using the iD5 for ATR measurements (diamond). The spectra were recorded in transmission mode in a wavenumber range 4000–500 cm^{-1}.

UV-Vis absorption spectra were acquired using Analytik Jena Specord 50 spectrophotometer. Luminescence spectrum of FITC-conjugated UCNPs was obtained following excitation at λ = 470 nm on a PerkinElmer LS 50 luminescence spectrometer, equipped with a Xenon lamp source.

The steady state upconversion luminescence measurements were performed with a wavelength tunable short pulsed Ti:sapphire laser system (Mai Tai HP, Spectra-Physics, Mountain View, CA, USA). The output from the Ti:sapphire laser consists of 150 fs pulses at a repetition rate of 80 ± 1 MHz. The spectra were detected using ICCD camera (Horiba) cooled to -5 °C. For time-resolved measurements, a Sunlite laser (continuum source, 250 mW) with a laser wavelength of 793 nm was used for excitation. The emitted light was spectrally decomposed (100 lines/mm) by iHR 550 Horiba spectrometer (slot width 200 μm). The central wavelength of the spectrometer was set to 520 nm, and spectra were recorded in the range 370–670 nm. The spectra were detected by an ICCD camera cooled to -5 °C (Horiba). A dynamic step width was used to describe species with a long emission life time as well as species with short emission life time.

Synthesis

Erbium-doped core UCNPs ($UCNP_{core,Nd}$ = β-$NaYF_4$:Nd^{3+}/Yb^{3+}/Er^{3+}(1/20/2%)). Hexagonal phase (β) $NaYF_4$ (2 mol% Er^{3+}, 1 mol% Nd^{3+})-doped hydrophobic nanocrystals were synthesised following procedure recently reported by our group.[52] Briefly, a mixture of YCl_3 (0.77 mmol), $NdCl_3$ (0.01 mmol), $YbCl_3$ (0.2 mmol) and $ErCl_3$ (0.02 mmol), oleic acid (8 mL), and Therminol® 66 (12 mL) was heated to 120 °C under vacuum for 45 min. Thereafter, the reaction solution was cooled to 90 °C with an argon stream. To this solution, ammonium fluoride (4 mmol) and sodium oleate (2.5 mmol) were added and the mixture stirred for 30 min under argon. Subsequently the reaction was heated to 318 °C (~10 °C/min) under argon and the reaction temperature was maintained for additional 10 min. Sub-10 nm erbium-doped core $NaYF_4$ UCNPs were precipitated out by the addition of ethanol, collected by centrifugation, and washed with ethanol several times, prior to their re-dispersion in hexane and storage at r.t until further use. The molar composition of lanthanide ions in final UCNP

samples was determined by inductively coupled plasma mass spectrometry (ICP-MS), which showed good agreement with stoichiometric ratios used for the synthesis.

Core-shell UCNPs ($UCNP_{core,Nd}$@$NaYF_4$:Nd^{3+}(25%)). Synthesis of hexagonal phase (β) $NaYF_4$ (2 mol% Er^{3+}, 2 mol% Nd^{3+}) core–shell nanocrystals were carried out following our previously reported method,[52] using a shell precursor solution made from T66 (8 mL), OA (4 mL), YCl_3 (0.65 mmol), $NdCl_3$ (0.25 mmol). The shell growth was performed directly on the earlier synthesised core UCNPs (60 mg). A solution of core UCNPs in 20 mL of T66/OA (3:2 v/v) was heated at 75 °C for 30 min under an argon atmosphere. While maintaining the inert atmosphere, the reaction temperature was elevated to 305 °C. Subsequently, the shell precursor solution was added dropwise (2 mL/h) using a peristaltic syringe pump. Afterwards, the reaction temperature was kept constant at 305 °C for 5 min before cooling down to 75 °C. Following the purification steps described for the core UCNPs (vide supra), sub-10 nm core-shell UCNPs were obtained. The molar composition of lanthanide ions in UCNP samples was determined ICP-MS, which showed good agreement with stoichiometric ratios used for the synthesis.

Surface coating of UCNPs with OPLT, PEG-phosphate, and alendronic acid.

Hydrophilic UCNPs were prepared through a two-step ligand exchange process using BF_4^- as an intermediate ligand.[59] The oleate ligands of core-shell UCNPs were first replaced with BF_4^- ions following a procedure reported by Dong et al.[59] For this, 3 mL of stock solution of core-shell UCNPs in hexane (10 mg/mL) was mixed with $NOBF_4$ (30 mg) in DMF (3 mL), and the biphasic solution was stirred vigorously for 10 min at room temperature allowing an extraction of BF_4^--coated nanoparticles from the upper hexane phase into the lower DMF phase. The BF_4^--coated UCNPs were then precipitated from the DMF solution using chloroform (2×20 mL) and collected after centrifugation (23830 × g, 15 min). Afterwards, the transparent pellet was once again dispersed in 5 mL of DMF and centrifuged (1000 × g; 3 min) to remove any larger aggregates, and the supernatant was used as a stock solution for all subsequent hydrophilic coating procedures.

In the second step, the desired capping ligands (alendronic acid, PEG-phosphate or OPLT) were used as final stabilising agents. For the final coating the UCNPs with hydrophilic ligands, 1 mL of the stock dispersion of BF_4^--coated UCNPs was slowly added to a prepared aqueous solution (3 mL) of the corresponding ligand (25 mg in 3 mL of $NaHCO_3$ (1 M aqueous solution) for alendronate, 1 M NH_3/H_2O (1/2 v/v) for PEG-phosphate and OPLT) and stirred vigorously for 2 h. The turbid dispersion was centrifuged (2383 × g, 5 min), the supernatant was discarded and the resulting pellet was re-dispersed in water (500 µL) and centrifuged for 15 min at 2383 × g. This step was repeated twice. Finally, the pellet was re-dispersed in water (5 mL), and passed through a 30 kDa cut-off centrifuge tube filter (1000 × g, 30 min) to remove any low molecular weight impurities. The resulting dispersion was filtered through a 0.22 µm PTFE syringe filter (to remove any large aggregates) and stored at r.t until further use.

Surface functionalisation with fluorescein isothiocyanate

Fluorescein isothiocyanate (FITC) solution was prepared by dissolving 1 mg of the reactive dye in 1 mL of anhydrous dimethyl sulfoxide (DMSO). Then, 200 µL of alendronate-coated UCNPs (10 µg/µL in dd water) were mixed with 2, 4 or 8 µL of FITC solution in 20 µL of 100 mM carbonate buffer (pH 9.2). The mixture was slowly shaken at room temperature (in darkness) for up to 4 h, purified by spin ultrafiltration using 10 kDa cut-off centrifuge tube filters (5000 x g, 5 min) and then resuspended in dd water. The coupling reaction was monitored by thin layer chromatography (TLC), performed using glass microfiber chromatography paper impregnated with a silica gel (iTLC-SG) as stationary phase and a 1:2 (v/v) mixture of NH_4OAc (2 M)/MeOH as mobile phase. After TLC, images of the chromatography stripes were acquired with an Amersham Typhoon 5 Scanner (GE Healthcare) using the specific excitation/emission wavelength for CY2.

Isolation and characterisation of nanoparticle-protein complexes

Biomolecular corona forming on water-dispersible UCNP was isolated as described recently with slight modifications.[79] Briefly, samples containing a total amount of 100 µg of OPLT-, PEG-phosphate-, or alendronate-coated UCNPs (final concentration 1 µg/µL) were incubated with increasing concentrations of normal (without pretreatment) or heat-inactivated human serum, diluted with PBS, for 1 h at 37 °C or 4 °C in protein LoBind vials (Eppendorf). For heat inactivation, the human serum was incubated at 56 °C for 30 min prior to its addition to the different water-dispersible UCNPs. After incubation in serum, samples were centrifuged for 5 min at 8000 × g and 4 °C to pellet the UCNP-corona complexes and to remove the supernatant serum. The pellets were then washed three times with ice-cold PBS and centrifuged again for 5 min at 8000 × g and 4 °C to remove proteins with low affinity for the nanoparticle surface. Finally, the UCNP-corona pellets were air-dried after the last centrifugation step to evaporate remaining liquid, resuspended in Laemmli buffer supplemented with 355 mM β-mercaptoethanol and incubated for additional 5 min at 95 °C to reduce and denature the proteins. After cooling to room temperature, the samples were loaded on a 12% SDS-polyacrylamide gel and subjected to electrophoresis until the bromophenol blue dye of the sample buffer reached the end of the gel. After electrophoretic separation, the gels were stained with colloidal Coomassie G-250 (PageBlue Protein Staining Solution, Thermo Fisher Scientific) according to the manufacturer's instructions.

Conflicts of interest

There are no conflicts to declare.

Acknowledgements

We thank Dr Astrid Barkleit (Institute of Resource Ecology, HZDR) for her support with the time-resolved luminescence spectroscopy measurements. This work was supported by the Helmholtz Initiative and Networking Fund (Functional Nanomaterials for Multimodality Cancer Imaging (NanoTracking), project ID: VH-VI-421), a HZDR fellowship to M.S., a Marie Curie International Outgoing Fellowship (Grant 627113) to M.K., and an Alexander von Humboldt Foundation research fellowship to T.J.

Notes and references

1. F. Auzel, *Chem. Rev.*, 2004, **104**, 139-173.
2. L. Prodi, E. Rampazzo, F. Rastrelli, A. Speghini and N. Zaccheroni, *Chem. Soc. Rev.*, 2015, **44**, 4922-4952.
3. B. Zhou, B. Shi, D. Jin and X. Liu, *Nat. Nanotechnol.*, 2015, **10**, 924-936.
4. G. Y. Chen, H. L. Qju, P. N. Prasad and X. Y. Chen, *Chem. Rev.*, 2014, **114**, 5161-5214.
5. A. Gnach, T. Lipinski, A. Bednarkiewicz, J. Rybka and J. A. Capobianco, *Chem. Soc. Rev.*, 2015, **44**, 1561-1584.
6. S. H. Nam, Y. M. Bae, Y. I. Park, J. H. Kim, H. M. Kim, J. S. Choi, K. T. Lee, T. Hyeon and Y. D. Suh, *Angew. Chem. Int. Ed.*, 2011, **50**, 6093-6097.
7. S. W. Wu, G. Han, D. J. Milliron, S. Aloni, V. Altoe, D. V. Talapin, B. E. Cohen and P. J. Schuck, *Proc. Natl. Acad. Sci. U. S. A.*, 2009, **106**, 10917-10921.
8. M. Haase and H. Schafer, *Angew. Chem Int. Ed.*, 2011, **50**, 5808-5829.
9. D. Kim, N. Lee, Y. I. Park and T. Hyeon, *Bioconjugate Chem.*, 2017, **28**, 115-123.
10. R. R. Anderson and J. A. Parrish, *J. Invest. Dermatol.*, 1981, **77**, 13-19.
11. R. Weissleder, *Nat. Biotechnol.*, 2001, **19**, 316.
12. V. Ntziachristos, *Nat. Methods*, 2010, **7**, 603-614.
13. Q. Xiao, Y. Ji, Z. Xiao, Y. Zhang, H. Lin and Q. Wang, *Chem. Commun.*, 2013, **49**, 1527-1529.
14. C. T. Xu, N. Svensson, J. Axelsson, P. Svenmarker, G. Somesfalean, G. Chen, H. Liang, H. Liu, Z. Zhang and S. Andersson-Engels, *Appl. Phys. Lett.*, 2008, **93**, 171103.
15. L. Wang, M. S. Draz, W. Wang, G. Liao and Y. Xu, *J. Biomed. Nanotechnol.*, 2015, **11**, 325-333.
16. H. Dong, S.-R. Du, X.-Y. Zheng, G.-M. Lyu, L.-D. Sun, L.-D. Li, P.-Z. Zhang, C. Zhang and C.-H. Yan, *Chem. Rev.*, 2015, **115**, 10725-10815.
17. X. Liu, C.-H. Yan and J. A. Capobianco, *Chem. Soc. Rev.*, 2015, **44**, 1299-1301.
18. X. Zhu, Q. Su, W. Feng and F. Li, *Chem. Soc. Rev.*, 2017, **46**, 1025-1039.
19. G. Chen, H. Qiu, P. N. Prasad and X. Chen, *Chem. Rev.*, 2014, **114**, 5161-5214.
20. A. Escudero, A. I. Becerro, C. Carrillo-Carrión, N. O. Núñez, M. V. Zyuzin, M. Laguna, D. González-Mancebo, M. Ocaña and W. J. Parak, *Nanophotonics*, 2017, **6**, 881.
21. Z. J. Gu, L. Yan, G. Tian, S. J. Li, Z. F. Chai and Y. L. Zhao, *Adv. Mater.*, 2013, **25**, 3758-3779.
22. Y. Liu, D. Tu, H. Zhu and X. Chen, *Chem. Soc. Rev.*, 2013, **42**, 6924-6958.
23. U. Resch-Genger and H. H. Gorris, *Anal. Bioanal. Chem.*, 2017, **409**, 5855-5874.
24. V. Muhr, S. Wilhelm, T. Hirsch and O. S. Wolfbeis, *Acc. Chem. Res.*, 2014, **47**, 3481-3493.
25. K. Zarschler, L. Rocks, N. Licciardello, L. Boselli, E. Polo, K. Pombo-Garcia, L. De Cola, H. Stephan and K. A. Dawson, *Nanomedicine: Nanotechnology, Biology and Medicine*, 2016, **12**, 1663-1701.
26. S. Wilhelm, M. Kaiser, C. Wurth, J. Heiland, C. Carrillo-Carrion, V. Muhr, O. S. Wolfbeis, W. J. Parak, U. Resch-Genger and T. Hirsch, *Nanoscale*, 2015, **7**, 1403-1410.
27. J. Zhou, Z. Liu and F. Li, *Chem. Soc. Rev.*, 2012, **41**, 1323-1349.
28. S. C. Baetke, T. Lammers and F. Kiessling, *Br. J. Radiol.*, 2015, **88**, 20150207.
29. Z. M. Lin, N. A. Monteiro-Riviere and J. E. Riviere, *Wiley Interdiscip. Rev.-Nanomed. Nanobiotechnol.*, 2015, **7**, 189-217.
30. A. Albanese, P. S. Tang and W. C. W. Chan, in *Annual Review of Biomedical Engineering, Vol 14*, ed. M. L. Yarmush, Annual Reviews, Palo Alto, 2012, vol. 14, pp. 1-16.
31. E. Blanco, H. Shen and M. Ferrari, *Nat. Biotechnol.*, 2015, **33**, 941-951.
32. A. E. Nel, L. Mädler, D. Velegol, T. Xia, E. M. V. Hoek, P. Somasundaran, F. Klaessig, V. Castranova and M. Thompson, *Nat. Mater.*, 2009, **8**, 543.
33. N. Feliu, D. Docter, M. Heine, P. Del Pino, S. Ashraf, J. Kolosnjaj-Tabi, P. Macchiarini, P. Nielsen, D. Alloyeau, F. Gazeau, R. H. Stauber and W. J. Parak, *Chem. Soc. Rev.*, 2016, **45**, 2440-2457.
34. T. Lammers, F. Kiessling, W. E. Hennink and G. Storm, *J. Control. Release*, 2012, **161**, 175-187.
35. M. P. Monopoli, C. Åberg, A. Salvati and K. A. Dawson, *Nat. Nanotechnol.*, 2012, **7**, 779.
36. Y. K. Lee, E. J. Choi, T. J. Webster, S. H. Kim and D. Khang, *Int. J. Nanomed.*, 2015, **10**, 97-112.
37. D. Docter, D. Westmeier, M. Markiewicz, S. Stolte, S. K. Knauer and R. H. Stauber, *Chem. Soc. Rev.*, 2015, **44**, 6094-6121.
38. R. van der Meel, T. Lammers and W. E. Hennink, *Exp. Opin. Drug Deliv.*, 2017, **14**, 1-5.
39. A. Wicki, D. Witzigmann, V. Balasubramanian and J. Huwyler, *J. Control. Release*, 2015, **200**, 138-157.
40. J. Shi, P. W. Kantoff, R. Wooster and O. C. Farokhzad, *Nat. Rev. Cancer*, 2017, **17**, 20-37.
41. J. Nam, N. Won, J. Bang, H. Jin, J. Park, S. Jung, S. Jung, Y. Park and S. Kim, *Adv. Drug Deliv. Rev.*, 2013, **65**, 622-648.
42. A. Vonarbourg, C. Passirani, P. Saulnier and J. P. Benoit, *Biomaterials*, 2006, **27**, 4356-4373.
43. F. Alexis, E. Pridgen, L. K. Molnar and O. C. Farokhzad, *Mol. Pharm.*, 2008, **5**, 505-515.
44. K. Knop, R. Hoogenboom, D. Fischer and U. S. Schubert, *Angew. Chem. Int. Ed.*, 2010, **49**, 6288-6308.
45. J. S. Suk, Q. Xu, N. Kim, J. Hanes and L. M. Ensign, *Adv. Drug Deliv. Rev.*, 2016, **99**, 28-51.
46. K. Pombo-García, K. Zarschler, L. Barbaro, J. A. Barreto, W. O'Malley, L. Spiccia, H. Stephan and B. Graham, *Small*, 2014, **10**, 2516-2529.
47. M. Mahmoudi, N. Bertrand, H. Zope and O. C. Farokhzad, *Nano Today*, 2016, **11**, 817-832.
48. K. Pombo-García, C. L. Rühl, R. Lam, J. A. Barreto, C. S. Ang, P. J. Scammells, P. Comba, L. Spiccia, B. Graham, T. Joshi and H. Stephan, *ChemPlusChem*, 2017, **82**, 638-646.
49. K. Pombo-García, S. Weiss, K. Zarschler, C.-S. Ang, R. Hübner, J. Pufe, S. Meister, J. Seidel, J. Pietzsch, L. Spiccia, H. Stephan and B. Graham, *ChemNanoMat*, 2016, **2**, 959-971.
50. D. F. Moyano, K. Saha, G. Prakash, B. Yan, H. Kong, M. Yazdani and V. M. Rotello, *ACS Nano*, 2014, **8**, 6748-6755.
51. R. Naccache, Q. Yu and J. A. Capobianco, *Adv. Opt. Mater.*, 2015, **3**, 482-509.
52. J. Hesse, D. T. Klier, M. Sgarzi, A. Nsubuga, C. Bauer, J. Grenzer, R. Hübner, M. Wislicenus, T. Joshi, M. U. Kumke and

H. Stephan, *ChemistryOpen*, 2018, **in press**, DOI: 10.1002/open.201700186.
53. Z.-Y. Yang, S.-L. Luo, H. Li, S.-W. Dong, J. He, H. Jiang, R. Li and X.-C. Yang, *RSC Adv.*, 2014, **4**, 59965-59969.
54. L. Sandiford, A. Phinikaridou, A. Protti, L. K. Meszaros, X. Cui, Y. Yan, G. Frodsham, P. A. Williamson, N. Gaddum, R. M. Botnar, P. J. Blower, M. A. Green and R. T. M. de Rosales, *ACS Nano*, 2013, **7**, 500-512.
55. M. R. Mirza, M. Rainer, C. B. Messner, Y. Guzel, D. Schemeth, T. Stasyk, M. I. Choudhary, L. A. Huber, B. M. Rode and G. K. Bonn, *Analyst*, 2013, **138**, 2995-3004.
56. P. Cao, L. Tong, Y. Hou, G. Zhao, G. Guerin, M. A. Winnik and M. Nitz, *Langmuir*, 2012, **28**, 12861-12870.
57. A.-A. Guay-Bégin, P. Chevallier, L. Faucher, S. Turgeon and M.-A. Fortin, *Langmuir*, 2012, **28**, 774-782.
58. J.-C. Boyer, M.-P. Manseau, J. I. Murray and F. C. J. M. van Veggel, *Langmuir*, 2010, **26**, 1157-1164.
59. A. Dong, X. Ye, J. Chen, Y. Kang, T. Gordon, J. M. Kikkawa and C. B. Murray, *J. Am. Chem. Soc.*, 2011, **133**, 998-1006.
60. N. G. Connelly and W. E. Geiger, *Chem. Rev.*, 1996, **96**, 877-910.
61. S. N. Achary, S. Bevara and A. K. Tyagi, *Coord. Chem. Rev.*, 2017, **340**, 266-297.
62. J. Clogston and A. K Patri, in *Characterization of Nanoparticles Intended for Drug Delivery. Methods in Molecular Biology (Methods and Protocols)*, ed. S. McNeil, Humana Press, 2011, vol. 697, pp. 63-70.
63. Z. G. Estephan, J. A. Jaber and J. B. Schlenoff, *Langmuir*, 2010, **26**, 16884-16889.
64. Y. Liang, N. Hilal, P. Langston and V. Starov, *Adv. Colloid Interface Sci.*, 2007, **134-135**, 151-166.
65. R. Arppe, I. Hyppanen, N. Perala, R. Peltomaa, M. Kaiser, C. Wurth, S. Christ, U. Resch-Genger, M. Schaferling and T. Soukka, *Nanoscale*, 2015, **7**, 11746-11757.
66. E. V. Samsonova, A. V. Popov, A. S. Vanetsev, K. Keevend, K. Kaldvee, L. Puust, A. E. Baranchikov, A. V. Ryabova, S. G. Fedorenko, V. Kiisk, I. Sildos, J. Kikas, R. Steiner, V. B. Loschenov and Y. V. Orlovskii, *J. Lumin.*, 2016, **169**, 722-727.
67. A. Beeby, I. M. Clarkson, R. S. Dickins, S. Faulkner, D. Parker, L. Royle, A. S. de Sousa, J. A. Gareth Williams and M. Woods, *J. Chem. Soc., Perkin Trans. 2*, 1999, 493-504.
68. X. Wang and D. Jia, in *Phosphor handook*, eds. W. M. Yen, S. Shionoya and H. Yamamoto, CRC Press/Taylor and Francis, 2 edn., 2007.
69. A. J. J. Bos, *Radiat. Meas.*, 2006, **41**, S45-S56.
70. L. Hu, Y. Fan, L. Liu, X. Li, B. Zhao, R. Wang, P. Wang, A. M. El-Toni and F. Zhang, *Adv. Opt. Mater.*, 2017, **5**, 1700680-n/a.
71. J. Yang, Y. Liu, Y. Zhao, Z. Gong, M. Zhang, D. Yan, H. Zhu, C. Liu, C. Xu and H. Zhang, *Chem. Mater.*, 2017, **29**, 8119-8131.
72. P. Zhao, W. Ji, S. Zhou, L. Qiu, L. Li, Z. Qian, X. Liu, H. Zhang and X. Cao, *Mater. Sci. Eng., C*, 2017, **79**, 191-198.
73. J.-C. G. Bunzli and S. V. Eliseeva, *Chem. Sci.*, 2013, **4**, 1939-1949.
74. Z. Junying, Z. Zhang, T. Wang and W. Hao, *Mater. Lett.*, 2003, **57**, 4315-4318.
75. P. Foroozandeh and A. A. Aziz, *Nanoscale Res. Lett.*, 2015, **10**, 221.
76. M. Mahmoudi, M. A. Shokrgozar and S. Behzadi, *Nanoscale*, 2013, **5**, 3240-3244.
77. M. Mahmoudi, A. M. Abdelmonem, S. Behzadi, J. H. Clement, S. Dutz, M. R. Ejtehadi, R. Hartmann, K. Kantner, U. Linne, P. Maffre, S. Metzler, M. K. Moghadam, C. Pfeiffer, M. Rezaei, P. Ruiz-Lozano, V. Serpooshan, M. A. Shokrgozar, G. U. Nienhaus and W. J. Parak, *ACS Nano*, 2013, **7**, 6555-6562.
78. G. R. Kieczykowski, R. B. Jobson, D. G. Melillo, D. F. Reinhold, V. J. Grenda and I. Shinkai, *J. Org. Chem.*, 1995, **60**, 8310-8312.
79. K. Pombo-García, K. Zarschler, J. A. Barreto, J. Hesse, L. Spiccia, B. Graham and H. Stephan, *RSC Adv.*, 2013, **3**, 22443.

SYNOPSIS

Hide and Seek. Surface modification of hydrophobic β-$NaYF_4$ upconverting nanoparticles (UCNPs) with alendronic acid, a strongly binding di-phosphonate ligand, produces water-

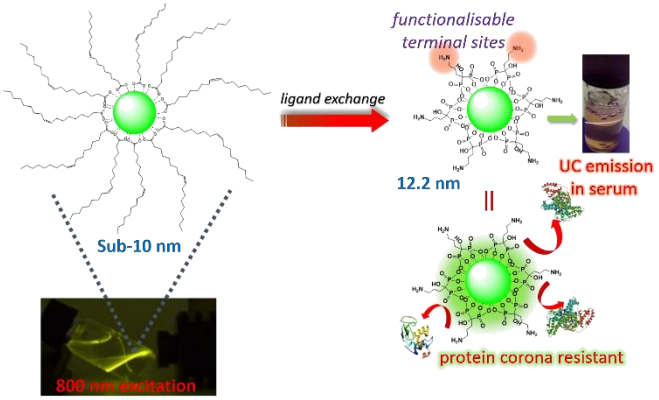

dispersible UCNPs, without major increases in particle size. These UCNPs display high colloidal stability, are protein corona resistant, exhibit bright upconversion luminescence (800 nm excitation), and are ready for incorporating multiple targeting, therapeutic and imaging moieties.